PIC simulations of RF sheaths with non-adiabatic electrons

Léonel Tsowémoo Faabomvé*, *Guillaume* Urbanczyk, *Stéphane* Heuraux, and *Jérôme* Moritz

Institut Jean Lamour - CNRS - Université de Lorraine.
Campus Artem 2 allée André Guinier BP 50840 54011 Nancy Cedex – France.

Abstract. This study investigates the dynamics of radio-frequency (RF) sheaths in magnetized plasmas, relevant to Ion Cyclotron Resonance Heating (ICRH) systems in fusion devices. Using a 1D3V Particle-In-Cell (PIC) model, we analyzed the rectification of the sheath potential and its dependence on the RF frequency and the magnetic field inclination with respect to the wall. Simulations reveal that grazing magnetic field angles significantly enhance the time-averaged sheath potential, sometimes exceeding the applied RF voltage due to increased electron transit times and residual charge buildup. These effects are most pronounced for RF frequencies between 1 and 5 times the ion cyclotron frequency. Additionally, we uncover a mechanism responsible for the enhancement of electron heating at grazing incidences, where electrons interact more frequently with the expanding sheaths and experience strong electric fields, leading to the formation of energetic electron bursts. This acceleration is linked to the observed increase in rectified potential and may have critical implications for material sputtering and impurity generation on ICRF antenna surfaces.

Introduction

In both present and future reactors, it has been shown both numerically and experimentally [1, 2] that one of the main heating systems will be Ion cyclotron Resonant heating (ICRH). It is the only mechanism that heat ions directly, and the absence of cut-off at higher density [3], is an advantage for heating all the way to the plasma core. These waves are launched from Ion Cyclotron Range of Frequency (ICRF) antennas located in high density region of current tokamaks to ensure a good coupling with the plasma core [4]. The design of antennas is such that the magnetic field lines intersect the limiters with various angles from large incidence to grazing ones, leading to different sheath behavior. The launched wave first interacts with the Scrape-Of-Layer (SOL) plasma and due to the difference in mobility between ions and electrons, a non-neutral space zone called the sheath [5] is formed closed to the antenna to balance ions and electrons flux reaching the antenna limiters. The more mobile particles (to connect from the sheath entrance to the wall) will dictate the sign of the sheath potential: electrons for a positive sheath potential, or ions for electro-negative sheath. Parameters such as the RF *frequency* ω and the direction of the magnetic field lines relative to the wall modify the particles mobility, which influences on the RF sheaths dynamics. This asymmetry in particles response in the sheath leads to sheath rectification, generating an average electric field from the oscillating applied potential. This drop of potential accelerates particles and leads to a significant energy flux deposited on the antennas structure [6, 7].

An approach to investigate RF sheaths is to use numerical simulations with a microscale model of a plasma discharge, using fluid or particular models [8, 9]. The RF sheath potential drop in the sheath is higher than that obtained from thermal (or Bohm) sheaths, V_{fl} (where $V_{fl} \approx 3T_e$ is the floating potential with T_e being the electron temperature). It has been shown [10] that the RF sheath can be treated as a succession of stationary states when the ratio of the ion plasma frequency to the RF frequency $\frac{\omega_{pi}}{\omega} \gg 1$. This corresponds to both ions and electrons that respond instantaneously to the modulations of the RF exciting source, which corresponds to the so-called quasi-static approximation. As ω increases, the previous ratio decreases, reducing ions mobility, so that when $\omega_{pi} \ll \omega < \omega_{pe}$, ions undergo an average electric field while electrons are still able to adapt the oscillating potential. In this situation however, the average sheath potential $\langle V_{DC} \rangle$ increases slightly. Notice that $\langle V_{DC} \rangle$ is a very important parameter in sheath dynamics because it determines the ability of incoming ions to exceed the sputtering threshold of the antenna material, which could lead to plasma contamination. In the presence of a magnetic field $\mathbf{B}$ tilted relative to the powered surface, the mobility of charged particles is altered, particularly for electrons, which are constrained to follow the magnetic field lines toward the antenna. Since the mobility of particles directly affects their transit time within the sheath, a strong influence of the magnetic field $\mathbf{B}$ incidence on the rectification properties is expected. This situation has already been investigated in the literature for large magnetic field incidences, assuming a Boltzmann equilibrium for electrons [8, 9, 11]. It has been shown in [12], however, that this last assumption no longer holds at grazing an-

*Correspond. author: leonel.tsowemoo-faabomve@univ-lorraine.fr

gles of the magnetic field, as the electron transit time is no longer negligible compared to the RF period. In this paper, we present a comprehensive analysis of sheath dynamics through Particle-In-Cell (PIC) simulations, where the trajectories of both ions and electrons are computed, even under grazing incidences of the magnetic field, where a non-adiabatic response has to be taken into account. In the first section, we introduce the system model. The second part is dedicated to a detailed discussion of the particle flux at the wall and the rectification effects, particularly in relation to RF *frequency* and the inclination of the magnetic field. Finally, in the third section, we explore the mechanisms by which electrons can be heated at grazing incidences, especially when their transit time through the sheath is comparable to the RF period, and examine how this influences the sheath potential drop.

1 PIC model

We performed RF simulations by using a custom-built 1D3V Particle-In-Cell (PIC) code with both kinetic ions (hydrogen) and electrons. The 2 eV plasma is confined between two parallel conductive electrodes, as described in [13] and shown on figure 1. The left electrode (referred to as the wall), assimilated either to a point on the antenna or to the connected chamber surface, is biased at $V_{wall} = V_{RF}\,sin(\omega t)$, with ω the RF frequency chosen in the range 0.1 to 5 Ω_i, in order to provide a broad overview of the dependence of sheath dynamics on RF frequency. We have investigated both ion cyclotron harmonic and non-harmonic resonances to disentangle the respective contributions of ions and electrons to sheath dynamics since it has been demonstrated that resonance sheath effects can modify the energy–angle distributions of ions impacting the walls [14].

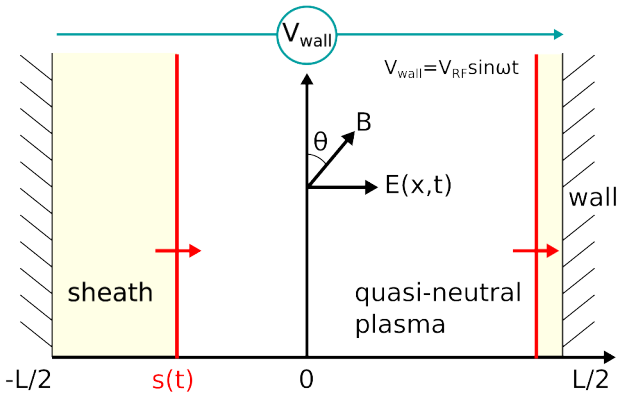

Figure 1. Symmetric 1D3V Particle-In-Cell model.

A potential of 0V is imposed on the right electrode, located $600\lambda_d$ away from the other; while the 0-peak amplitude V_{RF} is maintained at 100V in all simulations. A 3T magnetic field intersects the wall with angles θ between 1.25 (grazing) and 90° (normal incidence), and a central density of $n_0 = 10^{17}\mathrm{m}^{-3}$ is considered, giving rise to different values of $\frac{\omega_{pi}}{\omega}$, highlighted on table 1. Elastic collisions with neutral are also included in the simulations through a simple hard sphere model. The mean-free-path (λ_c) was calculated thanks to the elastic cross-section given in reference [15] at 2 eV with various neutral densities. Finally, the simulations are run for a large number of RF periods, typically ranging from 60 to 300, in order to reach a steady state behavior and capture the physics of RF sheaths in a well established regime.

Table 1. Ratio ω_{pi}/ω for different RF frequency at $10^{17}\mathrm{m}^{-3}$

$\frac{\omega_{pi}}{0.1\Omega_i}$	$\frac{\omega_{pi}}{\Omega_i}$	$\frac{\omega_{pi}}{2\Omega_i}$	$\frac{\omega_{pi}}{5\Omega_i}$
14.5	1.45	0.73	0.3

2 RF sheath properties

Figure 2 shows the angular variation of the rectified sheath potential $\langle V_{DC}\rangle$ for various RF *frequencies* (ω) and a mean-free-path of 7.08cm (neutral density of $10^{20}\mathrm{m}^{-3}$). This potential represents the time-averaged value of the oscillating voltage at the sheath edge. When the magnetic field is perpendicular to the surface, $\langle V_{DC}\rangle$ increases with ω, starting from a value close to $\frac{V_{RF}}{\pi}$, which corresponds to the average of a perfectly rectified sine wave, and approaching V_{rec}. The latter, approximately $\frac{V_{RF}}{2}$, is obtained using the following relation[11]

$$V_{rec} = \frac{T_e}{2} log(I_0\left(\frac{eV_{RF}}{T_e}\right) - V_{fl}$$

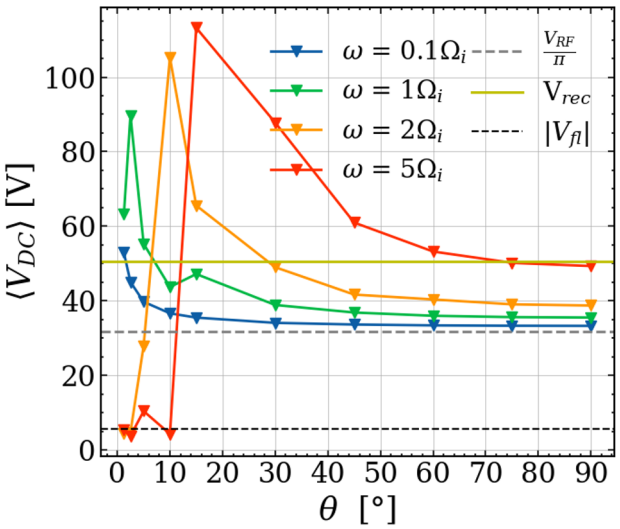

Figure 2. Angular variation of the rectified sheath potential $\langle V_{DC}\rangle$ for various RF *frequencies* (θ) and a mean-free-path of 7.08cm.

The transition between the two regimes is governed by the relationship between the particle transit time through the sheath and the RF period. At low frequencies, both ion and electron populations respond almost instantaneously to the RF field, adjusting accordingly. As ω increases, ions

experience an effective acceleration by the time-averaged potential drop, while electrons though still responsive to the RF oscillations require finite time to traverse the sheath and reach the wall in order to balance the particle flux once per period (and per wall). This results in a sinusoidal temporal variation of the electron density front, i.e., the sheath edge, and a slight increase in the time-averaged sheath potential compared to the ideal case of a perfectly rectified waveform. Interestingly, as the magnetic field incidence angle decreases, the electron transit time is expected to increase due to their confinement along magnetic field lines. This results in a significant rise in the sheath potential, with a pronounced peak occurring at angles between approximately 5° and 15° for RF frequencies in the range of 1 to 5 Ω_i. In some cases, the sheath potential can even exceed the amplitude of the applied RF voltage, figure 2. This phenomenon is observed for both resonant and non-resonant harmonics of Ω_i, indicating that it is primarily driven by electron inertia.

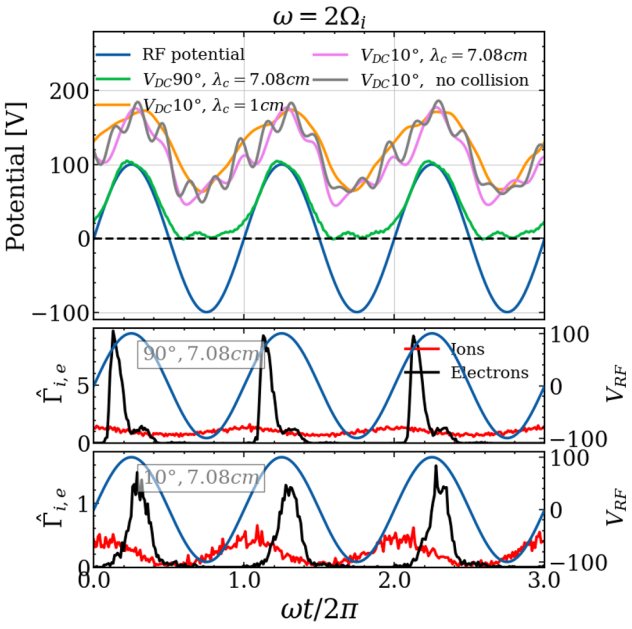

Figure 3. Top Panel: Time evolution of the plasma potential for two magnetic field inclinations and different collisionalities. Bottom Panel: Ion and electron fluxes ($\hat{\Gamma}_i, \hat{\Gamma}_e$) at the biased electrode, normalized to $n_0 C_s$, where n_0 is the plasma density and C_s is the Bohm velocity. The RF potential is overlaid in the figure (blue line) to visualize the phase of the cycle when particles leave the plasma.

Figure 3 shows the typical waveform recorded over multiple RF cycles at the center of the simulated plasma, for two different magnetic field inclinations, various mean free paths, and $\omega = 2\Omega_i$. At normal incidence (90°), the plasma potential closely follows a rectified sinusoidal waveform, as expected. However, when the magnetic field is tilted by just 10° relative to the wall, the plasma potential still exhibits a general sinusoidal shape but is noticeably shifted toward higher voltages. Superimposed high-frequency oscillations also appear, which tend to diminish as collisionality increases. The corresponding particle fluxes at the wall are also shown in Figure 3. At 90°, electrons reach the wall when the RF potential rises toward its maximum, but at grazing incidence, a significant delay is observed, attributable to the longer electron transit time. The transit time τ_e required for electrons to travel from the maximum sheath extent s to the wall can be estimated as $\tau_e = \frac{s}{v_{th} sin\theta}$, with v_{th} the electron thermal velocity. It can, under certain conditions (depending on the combination of ω and θ), become comparable to half the RF period τ_{RF}. This results in a residual sheath persisting even when the RF voltage returns to zero either mid-cycle or at the end of the cycle, as illustrated in Figures 4a and 4b. This behavior contrasts with what is observed at higher incidence angles (figure 4a). The presence of this residual sheath causes a sudden, significant voltage drop across the sheath, despite the wall potential being zero (V_{wall}=0). As a result, the time variation of the plasma potential experiences a vertical shift as shown in figure 3.

This behavior was already observed in [16], although no clear explanation was provided at the time.

Finally, when $\tau_e \gg \tau_{RF}$, electrons no longer respond to the RF field; they are effectively unable to adapt to its rapid variations. In this regime, the sheath potential drop becomes comparable to that observed under floating wall conditions (figure 2, θ<15° for 2 and 5 Ω_i).

3 Acceleration mechanism for electrons at grazing incidences

The superimposed oscillations observed in the time-varying plasma potential in Figure 3 are likely caused by bunches of hot electrons that are reflected and accelerated by the oscillating sheath, as illustrated in the $z - v_z$ phase diagram (Figure 5a). As collisionality increases, these hot electrons are progressively thermalized with the bulk population (Figure 5b), resulting in the gradual disappearance of the high-frequency plasma potential oscillations as depicted in Figure 3. Electron heating during RF discharges has been extensively studied in the literature [17–19] and is commonly referred to as stochastic. This mechanism involves the acceleration of electrons by the sheath and relies on several key assumptions: (i) electrons transit the sheath in a time much shorter than the RF period, and (ii) they reflect off the sheath edge, gaining energy when the sheath expands—an effect described by the hard-wall model [19, 20].

To gain a deeper understanding of the mechanism responsible for the observed electron acceleration in our case when $\tau_e \simeq \tau_{RF}$, we conducted additional ad hoc particle simulations using a step model for the electric field calculation. In this model, the ion density remains constant within the sheath, while the region is devoid of electrons. As a result, the electric field can be approximated as follows:

$$\begin{cases} E = \frac{n_0 e}{\epsilon_0}(z - s(t)) & \text{if} \quad z \leq s(t) \\ E = 0 & \text{if} \quad z > s(t) \end{cases}$$

Where s(t) is the sheath width defined as $s(t) = s_0 + s_0 sin(\omega t + \varphi)$. s_0 denotes the mean sheath thickness, set to 10 Debye lengths (λ_d), and the RF phase φ is randomly

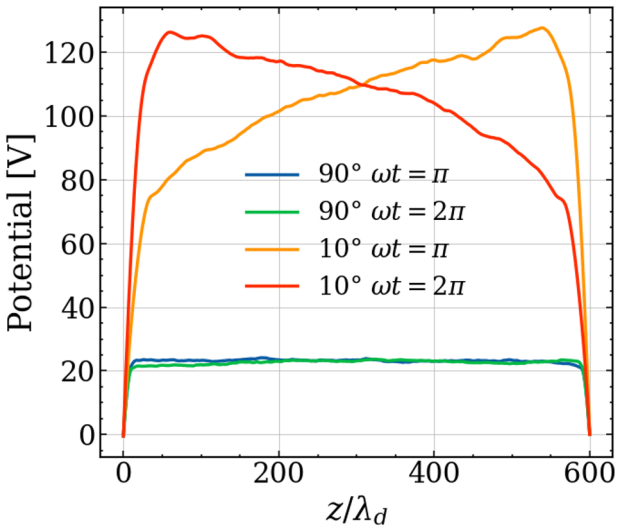

(a)

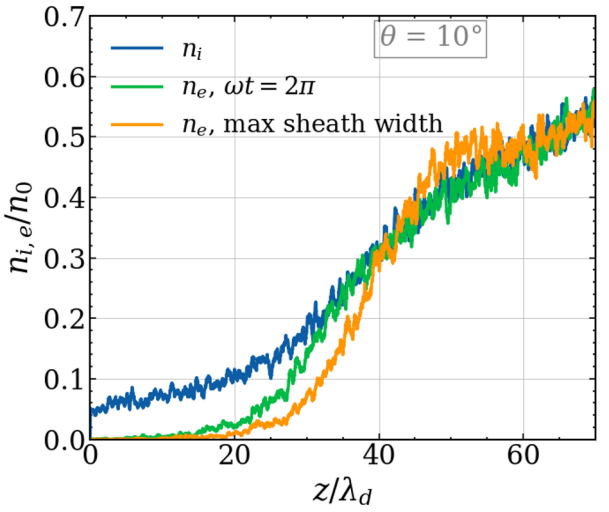

(b)

Figure 4. a) Snapshots of the plasma potential for two magnetic field orientations and at two different moments during the RF cycle (when the wall voltage returns to zero). b) Corresponding density profiles of ions and electrons. For electrons, the typical density profile when the sheath is fully extended is also shown.

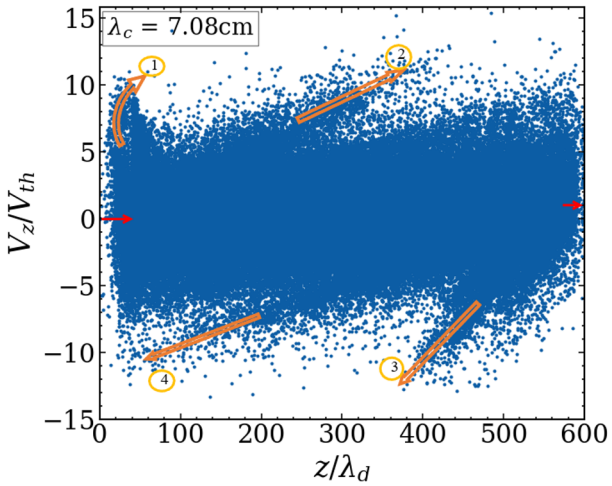

(a)

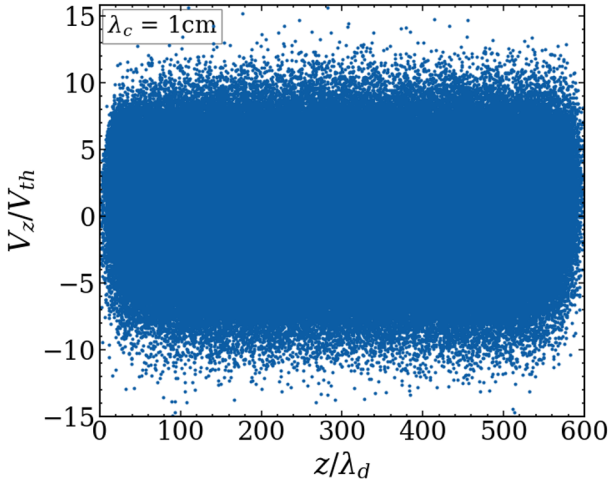

(b)

Figure 5. a) Phase diagram of electrons v_z versus z at ωt=x (when the sheath expands) for θ=10° and λ_c=7.08cm. The red arrows indicate the motion of the sheath. Burst 1 corresponds to electrons accelerated in the left sheath during the ongoing RF cycle when the sheath expands, while Burst 2 refers to electrons accelerated from the left sheath in the previous RF cycle. As the two sheaths oscillate back and forth, a similar scenario occurs on the right b) Same as in a), but for a mean free path of λ_c=1cm. Collisions cause the burst of accelerated electrons shown in panel a) to thermalize with the bulk electrons.

selected between 0 and 2π. Electrons are initially placed at $z = 3s_0$, slightly beyond the maximum sheath extent reached during an RF cycle. Their initial velocities are randomly drawn from a Maxwellian distribution for v_x and v_y, while a directed flux is imposed along the direction perpendicular to the wall (v_z). Electron trajectories are then computed at each time step until they either reach the wall or are reflected by the sheath and cross back beyond their starting position at $z = 3s_0$, where their final energy is recorded. Figure 6a presents typical trajectories for $\varphi = 0$, $\omega = 2\Omega_i$, and two magnetic field incidences: $\theta = 90°$ and 10°. For a perpendicular magnetic field inclination, electrons are reflected back by the sheath with a smaller (or larger) velocity when it collapses (or expands). Although the interaction time in this 90° case is very short, the electric field is weaker when the electron exits the sheath compared to when it enters, in the case of a collapsing sheath, which reduces its velocity. The opposite effect occurs when the sheath expands. In the case of a more grazing incidence, such as 10°, the time required for electrons to travel from the initial position to the electric field region means that they mostly encounter an expanding sheath. This results in a "shadowing effect," where a

significant portion of electrons are prevented from reaching the sheath during collapse, leading to a considerable average energy gain. Additionally, at grazing incidences, electrons penetrate deeper into the sheath, where they experience stronger electric fields and are reflected back into the plasma—unlike in the normal incidence case, where this effect is less pronounced. To quantify both the shadowing effect and the acceleration in the expanding sheath, we extracted from the simulations the phase φ_r of the RF cycle at which electrons reverse their direction within the sheath, that is, when their velocity component parallel to the magnetic field changes sign. Figure 6b shows the ratio of the outgoing to incoming electron energy, γ_E (the energy gained or lost in the sheath), as a function of φ_r for various magnetic field inclination angles. The shadowing effect previously introduced is clearly observed in this figure, as the range of accessible φ_r decreases with increasing B-field inclination. The absence of data points around $\varphi_r \simeq 0.5\pi$ for θ=90° and 15° corresponds to electron absorption by the wall (when the sheath has collapsed) and to the shadowing effect for 10°. Finally, this figure captures both key aspects of electron acceleration in the sheath: the enhanced energy gain at grazing incidences which can be of the order of 30 and the shadowing effect. This sheath acceleration mechanism helps explain the burst of fast electrons observed in the previous section, which contribute to the increased rectified potential for small field-wall angles.

4 Summary and conclusions

In this study, we have examined the angular dependence of the rectified sheath potential and the underlying mechanisms driving electron acceleration during RF discharges. Our findings reveal a strong correlation between the magnetic field orientation, RF frequency, and sheath potential, with a notable increase in the time-averaged potential as the magnetic field inclination decreases. At low angles, the electron transit time increases, leading to the buildup of residual space charge near the wall when the wall voltage returns to zero. This results in a significant rise in the average sheath potential, which can sometimes exceed the maximum applied RF voltage. This effect is particularly pronounced for RF frequencies in the range of 1 to 5 Ω_i, where the sheath potential exhibits a distinct peak between 5° and 15°. Moreover, we observe that at grazing incidences, electron heating and acceleration are significantly enhanced due to the combined effects of shadowing and the stronger electric fields encountered deeper within the sheath. We claim that these effects are linked to the observed burst of fast electrons in PIC simulations. These fast electrons can be thermalized through electron-neutral collisions, leading to an increase in plasma electron temperature and a further rise in the rectified potential at small field-wall angles.

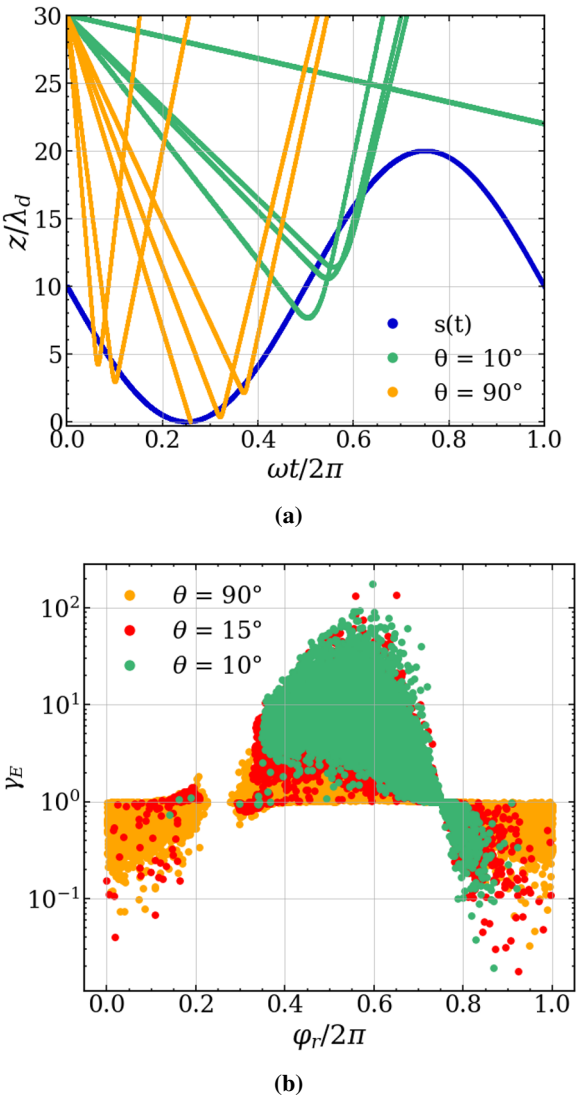

Figure 6. a) Trajectories of test particles for two different magnetic field inclinations. s(t) represents the motion of the sheath edge and defines the region with a strong electric field. b) The ratio of outgoing to incoming electron energy, γ_E, as a function of the phase φ_r at which particles are reflected by the sheath electric field.

Acknowledgements

This work was carried out within the framework of the EUROfusion Consortium, funded by the European Union via the Euratom Research and Training Programme (Grant Agreement No 101052200 — EUROfusion) and partly supported by the french PIA project « Lorraine Université d'Excellence », reference « ANR-15-IDEX-04-LUE.

References

[1] Y. Chen et al., Numerical study of minority ion heating scenarios in a spherical tokamak plasma, Phys. Plasmas **31**, 3 (2024). https://doi.org/10.1063/5.0187061

[2] Y.P. Zhao et al., EAST ion cyclotron resonance heating system for long pulse operation, Fusion Eng. Des. **89**, 11 (2014). https://doi.org/10.1016/j.fusengdes.2014.06.017

[3] J. Ongena et al., Recent advances in physics and technology of ion cyclotron resonance heating in view of future fusion reactors, Nucl. Fusion **59**, 5 (2017). https://iopscience.iop.org/article/10.1088/1361-6587/aa5a62/meta

[4] P. Manash Kumar et al., Plasma and antenna coupling characterization in ICRF-wall conditioning experiments, Fusion Eng. Des. **87**, 2 (2012). https://doi.org/10.1016/j.fusengdes.2011.10.009

[5] K.-U. Riemann, The Bohm criterion and sheath formation, J. Appl. Phys. **24**, 4 (1991). https://doi.org/10.1088/0022-3727/24/4/001

[6] R.A. Pitts et al., Plasma-wall interaction impact of the ITER re-baseline., Nucl. Mater. Energy **42**, 101854 (2025). https://doi.org/10.1063/1.5109256

[7] V. Bobkov et al., Impact of ICRF on the scrape-off layer and on plasma wall interactions: From present experiments to fusion reactor, Nucl. Mater. Energy **18**, 131-140 (2019). https://doi.org/10.1016/j.nme.2018.11.017

[8] H. Kohno, JR Myra, Investigation of two-dimensional radio-frequency sheath properties using a microscale fluid model. Nucl. Fusion **65**, 2 (2024). https://doi.org/10.1088/1741-4326/ad9c95

[9] M. Elias et al., Numerical model of the radio-frequency magnetic presheath including wall impurities, Phys. Plasmas **26**, 9 (2019). https://doi.org/10.1063/1.5109256

[10] P. Chabert, and N. Braithwaite, Physics of radio-frequency plasmas, (Cambridge University Press, 2011) pp 101-102

[11] K.-U. Riemann , Theoretical analysis of the electrode sheath in rf discharges, J. Appl. Phys. **65**, 3 (1989). https://doi.org/10.1063/1.343003

[12] E. Faudot et al., PIC simulation of the electron energy distribution function in a RF magnetized plasma column connected to a tilted electrode. AIP Conf. Proc., **2984**, 1 (2023). https://doi.org/10.1063/5.0162514

[13] J. Moritz et al., Sheath size and Child–Langmuir law in one dimensional bounded plasma system in the presence of an oblique magnetic field: PIC results, Phys. Plasmas **28**, 8 (2021). https://doi.org/10.1063/5.0055790

[14] M. Rezazadeh, J. R. Myra, D. Curreli, Resonance in radio frequency sheath admittance and enhanced impurity emission near the ion cyclotron frequency, Nucl. Fusion **63**, 126024 (2023). https://doi.org/10.1088/1741-4326/acee0e

[15] JS Yoon et al., Cross sections for electron collisions with hydrogen molecules, J. Phys. Chem. Ref. Data **37**, 913 (2008). https://pubs.aip.org/aip/jpr/article/37/2/913/916091

[16] S. Riyopoulos, Effects of static magnetic fields on rf-driven plasma sheaths, Phys. Plasmas **3**, 7 (1996). https://doi.org/10.1063/1.871969

[17] E. Kawamura et al., Stochastic heating in single and dual frequency capacitive discharges, Phys. Plasmas **13**, 5 (2006). https://pubs.aip.org/aip/pop/article/13/5/053506/1032342

[18] I.D. Kaganovich et al., Anomalous capacitive sheath with deep radio-frequency electric-field penetration, Physical Review Letters **89**, 26 (2002). https://doi.org/10.1103/PhysRevLett.89.265006

[19] M.A. Lieberman and A.J. Lichtenberg and SE Savas, Model of magnetically enhanced, capacitive RF discharges, IEEE Trans. Plasma. Sci. **19**, 189-196 (1991). https://doi.org/10.1109/27.106813

[20] M. Turner et al, Collisionless heating in radio-frequency discharges: a review, J. Appl. Phys. **42**, 19 (2009). https://doi.org/10.1088/0022-3727/42/19/194008